Available online at www.sciencedirect.com
SCIENCE DIRECT®
Journal of Solid State Chemistry 177 (2004) 2584–2590
JOURNAL OF SOLID STATE CHEMISTRY
http://elsevier.com/locate/jssc

Preparation of a highly active nanocrystalline TiO_2 photocatalyst from titanium oxo cluster precursor

Ling Wu, Jimmy C. Yu,* Lizhi Zhang, Xinchen Wang, and Wingkei Ho

Department of Chemistry, The Chinese University of Hong Kong, Shatin, New Territories, Hong Kong, China

Received 2 March 2004; accepted 30 March 2004

Abstract

Nanocrystalline TiO_2 (sample S1) was prepared from a titanium oxo cluster ($Ti_7O_4(OEt)_{20}$) precursor via a sol–gel route. This photocatalyst showed a higher photocatalytic activity than the TiO_2 (sample S2) obtained from titanium tetraisopropoxide. The samples were characterized by thermal analysis (TGA/DSC), X-ray diffraction, micro-Raman spectroscopy, transmission electron microscopy, N_2 adsorption (BET surface area), infrared absorption spectroscopy (FT-IR) and X-ray photoelectron spectroscopy. The characterization results show that both samples are anatase nanocrystals with particle sizes of about 12 nm, but the more photocatalytically active sample S1 has more surface hydroxyl groups and larger surface area and pore volume than sample S2.

Keywords: Nanocrystalline TiO_2; Titanium oxo cluster; Photocatalytic activity

1. Introduction

Nanocrystalline TiO_2 has extensive applications in solar energy conversion, catalysis and pollution treatment [1–4]. The photocatalytic activity of TiO_2 is greatly influenced by its crystal structure, particle size, surface area and the starting materials that the catalyst is derived from [5]. Furthermore, it has been found that the physical and chemical properties of nanocrystalline TiO_2 are strongly related to its preparation methods [6]. These include sonochemical [7], hydrothermal [8], flame combustion [9], microwave [10], nonhydrolytic [11] and sol–gel methods [12,13]. Titanium alkoxide and titanium chloride are often used as precursors in the preparation of TiO_2.

A number of titanium oxo clusters have been reported, with metal nuclearity ranging from 3 to 18 [14,15]. They can easily be obtained in a reproducible way by partly condensation and hydrolysis of titanium alkoxides in low water conditions. Their structures have been well determined with several $Ti–O_6$ octahedra in cage and terminal or bridging alkoxyls (ligands) in surface. These surface alkoxyls can react with nucleophilic species, but are less reactive when compared to those of titanium alkoxides [16]. Therefore, the hydrolysis and co-condensation rate of the titanium oxo clusters can be more easily controlled. The titanium oxo clusters with well-defined structure are able to act as nano-building blocks to assemble TiO_2 networks with high ordered architectures. For example, some of them were used to synthesize hybrid organic–inorganic networks with mesostructured titanium oxo [16] and the SiO_2–TiO_2 composite catalyst [17]. However, there is no report on the synthesis of nanocrystalline TiO_2 by using any titanium oxo cluster as the precursor.

Here, we report the use of a titanium oxo cluster $Ti_7O_4(OEt)_{20}$ precursor to prepare nanocrystalline TiO_2 (denoted as S1) by a sol–gel route. In comparison with TiO_2 obtained from titanium tetraisopropoxide as the precursor (denoted as S2), S1 showed higher photocatalytic activity on the oxidation of acetone in air. A reasonable explanation was described according to the characterization results of the samples.

*Corresponding author. Fax: +852-2603-5057.
E-mail address: jimyu@cuhk.edu.hk (J.C. Yu).

0022-4596/$ - see front matter © 2004 Elsevier Inc. All rights reserved.
doi:10.1016/j.jssc.2004.03.033

2. Experimental

2.1. Synthesis

All reagents were purchased from Aldrich. A titanium oxo solution was prepared by adding slowly 20 mmol of titanium tetraisopropoxide to a 30 mL solution of 20 mmol urea in absolute ethanol. The mixture in a beaker was covered with a piece of parafilm and sonicated in an ultrasonic bath for 1 h. The resulting solution was used in a subsequent sol–gel process. In a separate experiment, single crystals were allowed to grow from a titanium oxo solution over a period of several days. X-ray structure analysis on one of the tabular crystals shows that it is $Ti_7O_4(OEt)_{20}$.[1]

In the sol–gel process, a surfactant Pluronics triblock copolymer $(HO(CH_2CH_2O)_{20}(CH_2CH-(CH_3)O)_{70}(CH_2CH_2O)_{20}H$, P123) and a complexing agent acetylacetone (Hacac) were used to control the hydrolysis and condensation reaction. An absolute ethanol solution of P123 and Hacac was mixed with the titanium oxo solution under stirring. A 10% nitric acid was then added to the mixture. The molar ratios of the ingredients were as follows: titanium precursor/P123/acac/10% nitric acid/ethanol = 1:0.05:0.1:1.5:43. The final solution was stirred first for 6 h at room temperature, and then for 10 h at 50°C. The resulting sol was dried at 100°C for 12 h in air to form a xerogel. Finally, nanocrystalline TiO_2 (denoted sample S1) was obtained by the calcination of the xerogel at 500°C in air for 2 h. A reference nanocrystalline TiO_2 (denoted sample S2) was prepared by the same procedure but using titanium tetra-isopropoxide as a precursor.

2.2. Characterization

Thermalgravimetric analysis (TGA) and differential scanning calorimetry (DSC) were performed using a Netzsch STA 449C thermal analyzer, under air flow of 40 mL min^{-1} with a heating rate of 5°C min^{-1} from room temperature to 620°C. XRD patterns were obtained on a Bruker D8 Advance X-ray diffractometor with Cu$K\alpha$ radiation at a scan rate of 0.02° 2θ S^{-1}. Raman spectra of the powder samples on a glass slide were measured using a Renishaw 1000 micro-Raman system. Fifty times magnification objectives were selected. The excitation source used was an Argon ion laser operating at 514.5 nm with an output power of 20 mW. Transmission electron microscopy (TEM) images were taken on a Philips CM-120 electron microscopy instrument. The samples for TEM were prepared by dispersing the final powders in ethanol; the dispersion was then dropped on carbon–copper grids. The Brunauer–Emmett–Teller (BET) surface area (S_{BET}) and pore size distribution were determined using a Micromeritics ASAP 2010 nitrogen adsorption apparatus. All the samples were degassed at 180°C prior to BET measurements. Infrared (IR) spectra on pellets of the samples mixed with KBr were recorded on a Nicolet Magna 560 FTIR spectrometer at a resolution of 4 cm^{-1}. The concentration of the samples was kept at around 0.5%. X-ray photoelectron spectroscopy (XPS) measurements were done with a PHI Quantum 2000. XPS System with a monochromatic Al$K\alpha$ source and a charge neutralizer; all the binding energies were referenced to the C1*s* peak at 284.8 eV of the surface adventitious carbon.

2.3. Photocatalytic activity evaluation

Photocatalytic activities of the samples were evaluated by measuring the oxidation of acetone in air at room temperature using a 7000 mL reactor under a 15-W 365 nm UV lamp irradiation. The photocatalyst was prepared by dispersed 0.3 g of sample suspension in three dishes with 60 mm diameters. Temporal changes in the concentration of acetone, carbon dioxide and water vapor were monitored by a Photoacoustic IR Multigas Monitor. The detailed experiment was described in our previous papers [18].

3. Results and discussion

3.1. Preparation and single crystal structure of titanium oxo cluster precursor

Under the influence of ultrasound, titanium isopropoxide in the urea solution reacts with ethanol via nucleophilic substitution. Meanwhile, the isopropoxy groups in titanium isopropoxide are substituted gradually by ethanol, forming titanium ethoxide intermediate. The intermediate is then hydrolyzed and condensed to form $Ti_7O_4(OEt)_{20}$. The molecular structure of the titanium oxo cluster $Ti_7O_4(OEt)_{20}$ is shown in Fig. 1. The molecule consists of seven TiO_6 octahedra, the central octahedron sharing six surrounding polyhedra. The seven metal atoms are connected through three different kinds of oxygen bridges (two μ_4–O, two μ_3–O and eight μ–alkoxo groups) and 12 terminal alkoxo groups. The 12 terminal alkoxo and eight μ–alkoxo groups are reactive towards nucleophilic species; so further hydrolysis and co-condensation can go on to form TiO_2 networks in the sol–gel process.

[1] A suitable single crystal of $Ti_7O_4(OEt)_{20}$ was sealed under an inert atmosphere in a capillary and mounted on the goniometer head of a Siemens-Smart CCD diffractometer. The structure solution and refinement was performed using SHELXS-97 programs. Details concerning the crystallographic data collection and structure determination are given in the supporting material.

3.2. TGA-DSC thermal analysis

Results from thermogravimetric analysis (TGA) and DSC measurements can determine the optimum calcination temperature at which the organic template is removed and the inorganic phase is crystallized. Fig. 2a shows the TGA and DSC curves of the S1 xerogel sample. There are four features in the curves. The first weight loss of ca. 15% in the temperature range of 50–245°C is attributed to the loss of small molecular compounds, such as water and ethanol in the xerogel texture, corresponding to a gradual exothermic process from DSC curve. In the temperature range of 245–322°C, there is a second weight loss of about 50%, which corresponds to the decomposition of the block copolymer species (the $EO_{20}PO_{70}EO_{20}$). The decomposition of organic species also gives rise to a sharp exothermic peak at 322°C in the DSC curve. The third weight loss of ca. 12.5% in the range of 322–480°C is attributed to the gradual removal of the organic residues. The small exothermic peak at approximately 471°C is due to the amorphous–anatase transition of TiO_2. Finally, both TGA and DSC curves show little change in the range of 480–620°C. This indicates that the residues have been removed and a stable phase structure has been formed. These results confirm that the organic template can be effectively removed from the xerogel upon calcination at 500°C. The TGA and DSC curves of the S1 and S2 samples are shown, respectively, in Fig. 2b and c. TGA results show a 2.1% weight lost for both S1 and S2 due to the removal of physicosorption water.

3.3. Phase structure and particle size determination

The X-ray diffraction (XRD) patterns (Fig. 3) of the S1 and S2 samples show five distinctive TiO_2 peaks at

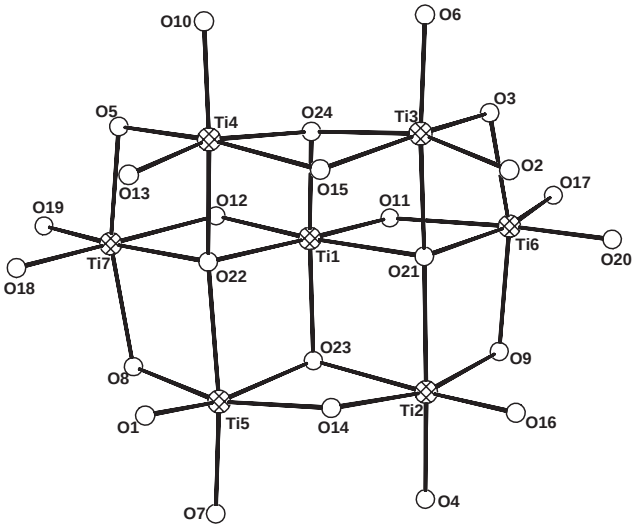

Fig. 1. Molecular structure of $Ti_7O_4(OEt)_{20}$. The carbon of ethoxy groups are omitted for clarity.

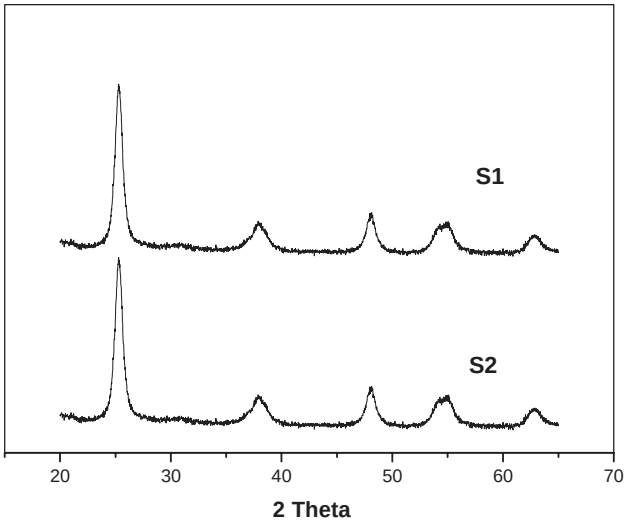

Fig. 3. XRD patterns of the TiO_2 samples.

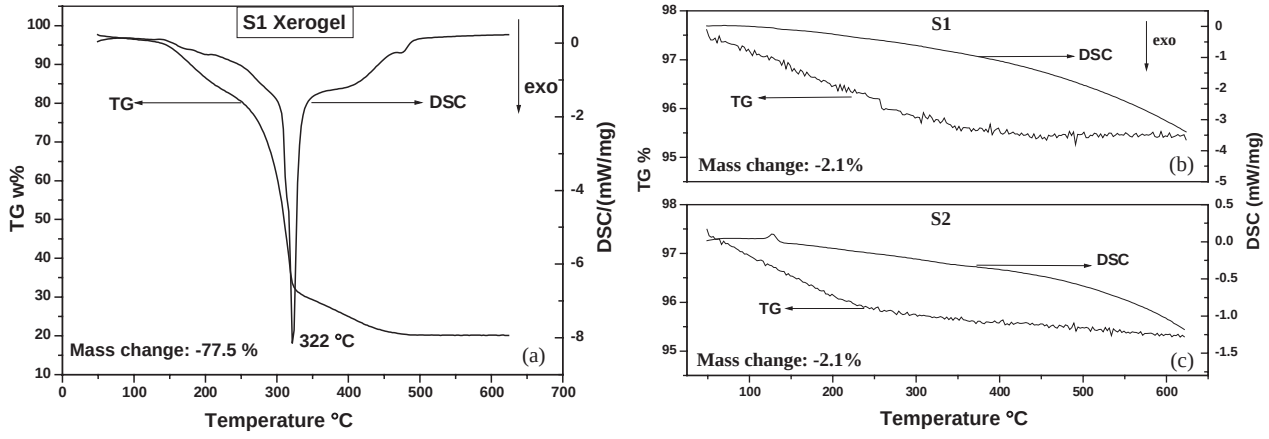

Fig. 2. TGA and DSC analysis of the S1 xerogel (a), S1 (b) and S2 (c) samples; the left *y*-axis represent the TGA lost weight data, and the right *y*-axis the DSC data.

25.33°, 37.92°, 48.03°, 54.58°, and 62.81°. These correspond to the anatase (101), (103, 004 and 112), (200), (105 and 211), (204) crystal planes (JCPDS 21-1272), respectively. The results of XRD patterns indicate that a pure anatase phase exists in the samples. The average crystallite sizes are 11.9 and 11.7 nm, respectively, for samples S1 and S2 (Table 1), as calculated by applying the Scherrer equation to the FWHM of the (101) crystal plane of anatase TiO_2.

Raman spectroscopy is more surface sensitive than XRD because an excitation energy in the near IR region is less penetrating than X-rays. A comparison of Raman spectroscopy with X-ray diffraction can be used to estimate the difference between the surface and bulk compositions of TiO_2 powders [19]. Titanium dioxide has three phase structures: anatase, rutile, and brookite. The three TiO_2 crystal structures have the same fundamental structural unit of $[TiO_6]$ octahedron but different modes of arrangement and links. Anatase is tetragonal ($I41/amd$) with two formula units per unit cell and six Raman active modes ($A_{1g} + 2B_{1g} + 3E_g$), whereas rutile (tetragonal, $P42/mnm$) has two units and four Raman active modes ($A_{1g} + B_{1g} + B_{2g} + E_g$). Brookite is orthorhombic ($Pcab$) with eight formula units per unit cell, and it shows 36 Raman active modes ($9A_{1g} + 9B_{1g} + 9B_{2g} + 9B_{3g}$) [20]. Since Raman spectroscopy is very sensitive to the phase structure of TiO_2, it can be used to identify surface structure of TiO_2 powders.

The Raman spectra of the TiO_2 samples S1 and S2 are shown in Fig. 4. Five peaks can be observed: a strong sharp peak at 144 cm^{-1}, three wide mid-intensity peaks at 398, 517, and 638 cm^{-1} and a weak peak at 196 cm^{-1}. The three bands at 638, 196, and 144 cm^{-1} are assigned to the E_g modes and the band at 398 cm^{-1} to the B_{1g} mode of the TiO_2 anatase phase. The band at 517 cm^{-1} is a doublet of A_{1g} and B_{1g} modes of TiO_2 anatase. These peak frequencies in the Raman spectra of the samples match those of literature [20]. These, together with the XRD results, confirm the samples S1 and S2 are single anatase phase that has long been considered as the most photocatalytically active form of titania.

The representative TEM images in Fig. 5 reveal that the nanoparticles in the S1 and S2 samples are uniform and monodisperse. The average diameter of the particles is estimated to be about 12 nm, in agreement with that obtained from XRD. These results indicate that the phase structure and size of the nanoparticles were not affected by the precursors.

3.4. Surface structure analysis

Fig. 6 shows pore size distribution curves calculated from the desorption branch of the nitrogen adsorption–desorption isotherms by the Barrett–Joyner–Halenda

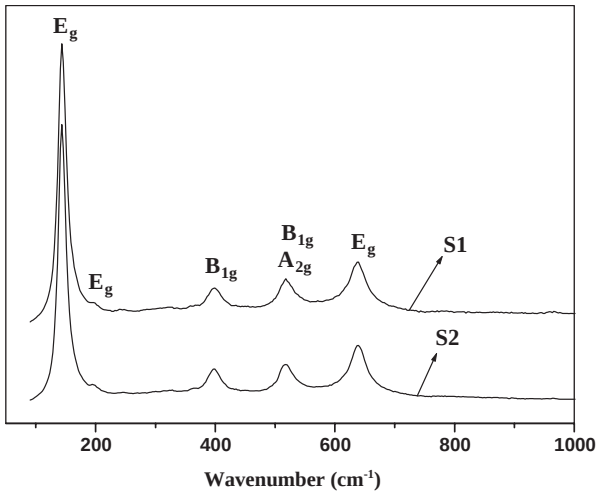

Fig. 4. Raman spectra of TiO_2 samples: S1(top) and S2(bottom).

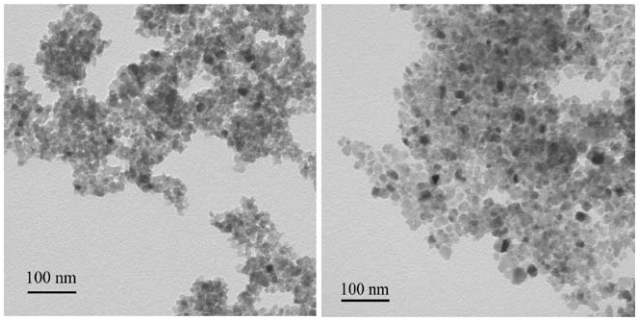

Fig. 5. TEM images of TiO_2 samples: S1(left) and S2(right).

Table 1
Summary of the physicochemical properties of the S1 and S2 samples

Samples	Crystalline size (nm)[a]	OH% in O 1*s*[b]	S_{BET} ($m^2 g^{-1}$)	Pore Size (nm)[c]	Pore volume ($cm^3 g^{-1}$)[d]	Activity, k (s^{-1}) (10^{-5})[e]
S1	11.9	21.6	117	7.3	0.275	7
S2	11.7	14.7	100	5.7	0.173	3.3

[a] Calculated by the Scherrer equation from the FWHM of the (101) crystal plane-based XRD data.
[b] Calculated by the peak areas of O 1*s* on XPS spectra.
[c] Estimated using the desorption branch of the isotherm.
[d] Single point adsorption total pore volume of pores at $P/P_0 = 0.975$.
[e] $k = -(\ln c/c_0)/t$, where k is the rate constant of acetone degradation; c is the acetone concentrate after 1 h degradation; c_0 is the initial acetone concentrate; t is the reaction time in seconds.

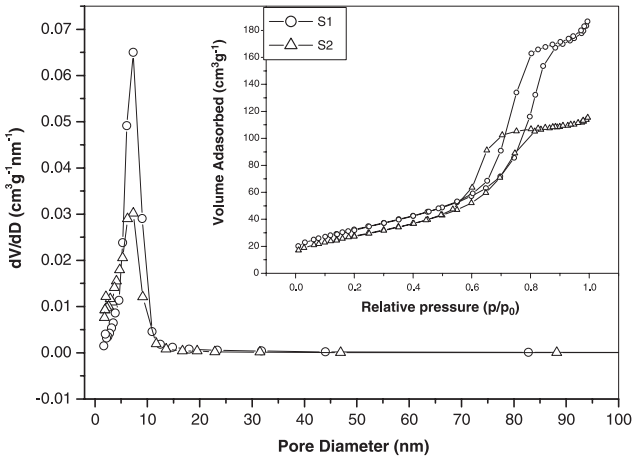

Fig. 6. N_2 adsorption–desorption isotherms (inset) and BJH pore size distributions: (○) S1 sample, and (△) S2 sample.

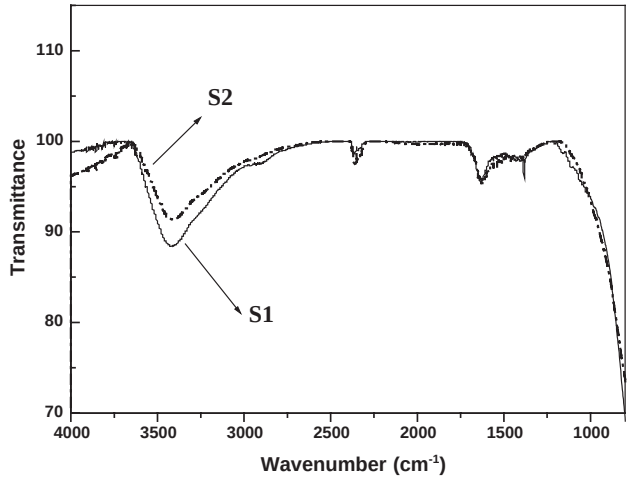

Fig. 7. FT-IR spectra of TiO_2 samples: solid line for S1 and dash line for S2.

(BJH) method and the corresponding isotherms (inset) of the samples. The sharp decline in desorption curves is an indication of mesoporosity [21]. The pore size distributions are narrow and centered around 7.3 and 6.8 nm for S1 and S2, respectively. The two samples have high surface areas and high pore volumes (Table 1). Meanwhile, the surface area and pore volume of S1 are higher than that of S2. That means the nanocrystalline TiO_2 prepared using the titanium oxo cluster have more surface active sites and channels readying for the chemisorption and diffusion of reactants.

Fig. 7 shows the FT-IR spectra of samples S1 and S2. Two absorption peaks are present in both spectra, one at 3420 cm^{-1} and the other around 1630 cm^{-1}. These correspond to the surface-adsorbed water and hydroxyl groups [22]. It should be noted that the peak at 3420 cm^{-1} for S1 sample is more intense than that for S2. Small characteristic CO_2 peaks at 2360 and 2337 cm^{-1} are also observed. Obviously, sample S1 prepared from the titanium oxo cluster can adsorb more water or hydroxyl groups than that of sample S2.

XPS measurements were carried out to determine the chemical composition of the prepared samples and the valence states of various species present therein. Fig. 8 (left) shows the XPS survey spectra of prepared TiO_2 samples. It can be observed that S1 and S2 contain only Ti, O, and C elements. The photoelectron peak for Ti 2*p* appears clearly at a binding energy 458.7 eV, O 1*s* at 530 eV and C 1*s* at 284.6 eV. No other photoelectron peak is observed. The peak positions are in agreement with literature values, which give O 1*s* and Ti $2p_{3/2}$ binding energies relative to TiO_2 species of 530 and 458.6 eV, respectively [23]. Fig. 8 (right) shows the high resolution XPS spectra of O 1*s* of the S1 and S2 samples. The regions of XPS spectra are composed of a narrow peak with a binding energy of ca. 530.0 eV (FWHM = 1.0 eV) and a broad peak with a binding energy of ca. 531.1 eV. The peaks with 530.0 and 531.1 eV can be, respectively, attributed to the Ti–O in TiO_2 and hydroxyl groups chemisorbed on the surface of the samples [21b,24]. The contributions of OH groups in O 1*s* on the samples are summarized in Table 1. It is interesting to note that the hydroxyl content in the S1 sample is higher than that in the S2 sample. We may thus conclude that compared to the titanium alkoxide precursors, the titanium oxo cluster can produce nanocrystalline TiO_2 with more surface hydroxyl groups in the sol–gel process. This may be attributed to the better-controlled hydrolysis and co-condensation as well as the larger block size of titanium oxo clusters [16].

3.5. Photocatalytic activity

Fig. 9a shows the degradation of acetone and evolution of carbon dioxide during photocatalysis. Over a 60 min period, the acetone concentrations decrease by 87 and 54 ppm for S1 and S2 samples, respectively. Corresponding increases in the concentration of CO_2 are also observed. The degradation rate constants for S1, S2 and the P25 standard are shown in Fig. 9b. The much higher photocatalytic activity of S1 can be explained by the TiO_2 photocatalysis mechanism [3,4,25]. Absorption of photons with energy greater than the band gap energy of TiO_2 results in the formation of conduction band electrons (e^-) and valence band holes (h^+), which can migrate toward the TiO_2 surface where the excited electrons can react with electron acceptors absorbed and the holes can be quickly converted to the hydroxyl radical upon oxidation of surface water or hydroxyl. The yield of hydroxyl radicals depends on the competition between oxidation of surface hydroxyl groups by the holes and electron–hole recombination. In the presence of oxygen as electron acceptor, the excited electrons can be scavenged by oxygen to form superoxide anion radicals. The latter produces hydrogen

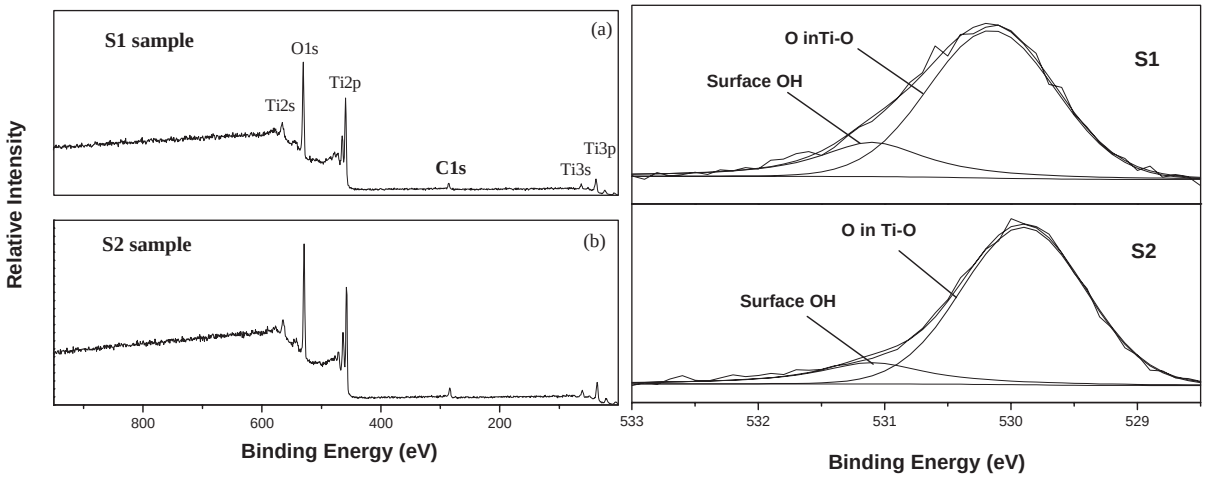

Fig. 8. XPS spectra of S1 and S2 samples (left) and high-resolution XPS spectra of the O 1*s* region for the samples (right).

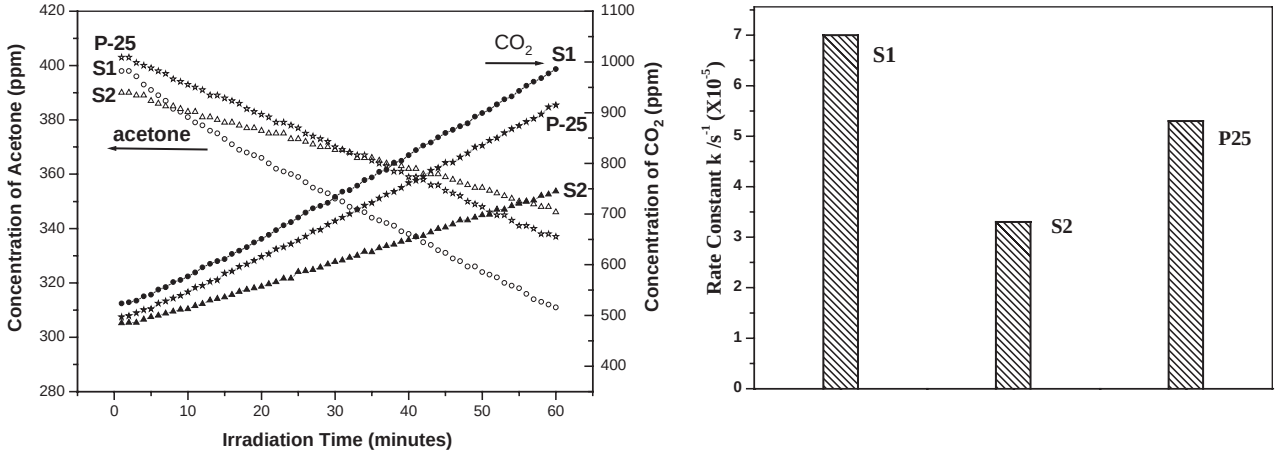

Fig. 9. (a) Concentration–time plots of acetone and CO_2 for S1, S2 samples and P25; and (b) the comparison of photocatalytic activities of S1, S2 samples and Degussa P25; $k = -(\ln c/c_0)/t$, where k is the rate constant of acetone degradation; c is the acetone concentrate after 1 h degradation; c_0 is the initial acetone concentrate; t is the reaction time in seconds.

peroxide by reacting with hydrogen ions, then the hydrogen peroxide can further produce hydroxyl radicals and hydroxyl anions by reacting with superoxide anion radicals and excited electrons. It is well known that the hydroxyl radical is a powerful oxidative agent which can destroy most organic pollutants. Therefore, depending on the properties of their surface hydroxyl groups, nanocrystalline TiO_2 can possess different photocatalytic activities. As observed from Table 1, S1 sample has the same crystal size as S2 sample, but S1 adsorbs 50% more hydroxyl groups than S2 does. The photocatalytic activity improvement of S1 is probably due to (1) the enhanced surface hydroxyl group adsorption, and (2) its larger surface area and pore volume. To compare with the commercial Degussa P25 TiO_2, it also can be seen in Fig. 9 that the photocatalytic activity of S1 sample prepared from titanium oxo cluster also exceeds that of Degussa P25.

In conclusion, nanocrystalline TiO_2 prepared from a new precursor $Ti_7O_4(OEt)_{20}$ exhibits high surface hydroxyl group content, large surface area and increased pore volume, resulting in much higher photocatalytic activity than that obtained from titanium tetraisopropoxide. As more members of the titanium oxo family become available [14,15], it would be interesting to conduct a systematic study on the new TiO_2 precursors.

Acknowledgments

The work was supported by the Research Grants Council (CUHK 4027/02P) and the Innovation and Technology Fund (ITS/118/01) of the Hong Kong Special Administrative Region.

References

[1] (a) M. Gratzel, Nature 414 (2001) 338;
(b) B. O'Regan, M. Gratzel, Nature 353 (1991) 737.

[2] (a) A. Fujishima, K. Hashimoto, T. Watanabe, Photocatalysis Fundamentals and Applications, 1st Edition, BKC, Tokyo, 1999;
(b) M. Kaneko, I. Okura, Photocatalysis, Science and Technology, Springer, Berlin, 2002.

[3] (a) N. Serpone, E. Pelizzetti, Photocatalysis: Fundamentals and Applications, Wiley, New York, 1989;
(b) D.F. Ollis, H. Al-Ekabi, Photocatalytic Purification and Treatment of Water and Air, Elsevier, Amsterdam, 1993.

[4] (a) M.A. Fox, M.T. Dulay, Chem. Rev. 93 (1993) 341;
(b) M.R. Hoffmann, S.T. Martin, W. Choi, D.W. Bahnemann, Chem. Rev. 95 (1995) 69;
(c) L. Linsebigler, G. Lu, J.T. Yates, Chem. Rev. 95 (1995) 735;
(d) A. Mills, R.H. Davies, D. Worsley, Chem. Soc. Rev. 22 (1993) 417.

[5] (a) K.L. Yeung, S.T. Yau, A.J. Maira, J.M. Coronado, J. Soria, P.L. Yue, J. Catal. 219 (2003) 107;
(b) C.B. Almquist, P. Biswas, J. Catal. 212 (2002) 145.

[6] (a) I. Justicia, P. Ordejon, G. Canto, J.L. Mozos, L. Fraxedas, G.A. Battiston, R. Gerbasi, A. Figueras, Adv. Mater. 14 (2002) 1399;
(b) Y.J. Liu, R.O. Claus, J. Am. Chem. Soc. 119 (1997) 5273.

[7] (a) J.C. Yu, J.G. Yu, W.K. Ho, L.Z. Zhang, Chem. Commun. (2001) 1942;
(b) J.C. Yu, L.Z. Zhang, J.G. Yu, New J. Chem. 26 (2002) 416;
(c) L.Z. Zhang, J.C. Yu, Chem. Commun. (2003) 1942;
(d) J.C. Yu, L.Z. Zhang, Z. Zheng, J.C. Zhao, Chem. Mater. 15 (2003) 2280.

[8] (a) J.C. Yu, L. Wu, J. Lin, P.S. Li, Q. Li, Chem. Commun. (2003) 1552;
(b) M. Andersson, L. Osterlund, S. Ljungstrom, A. Palmqvist, J. Phys. Chem. B 106 (2002) 10674.

[9] (a) S. Khan, M. Al-Shahry, W.B. Ingler, Science 297 (2002) 2243;
(b) D. Lee, S. Yang, M. Choi, Appl. Phys. Lett. 79 (2001) 2459.

[10] (a) T. Yamamoto, Y. Wada, H.B. Yin, T. Sakata, H. Mori, S. Yanagida, Chem. Lett. (2002) 964;
(b) G.J. Wilson, G.D. Will, R.L. Frost, S.A. Montgomery, J. Mater. Chem. 12 (2002) 1787.

[11] (a) H. Parala, A. Devi, R. Bhakta, R.A. Fischer, J. Mater. Chem. 12 (2002) 1625;
(b) T.J. Trentler, T.E. Denler, J.F. Bertone, A. Agrawal, V.L. Colvin, J. Am. Chem. Soc. 121 (1999) 1613.

[12] (a) S.A. Bilmes, P. Mandelbaum, F. Alvarez, N.M. Victoria, J. Phys. Chem. B 104 (2000) 9851;
(b) H.S. Yun, K. Miyazawa, H.S. Zhou, I. Honma, M. Kuwabara, Adv. Mater. 13 (2001) 1377;
(c) J. Livage, C. Sanchez, J. Non-Cryst. Solids 145 (1992) 11.

[13] (a) S. Roux, G.J. de, A.A. Soler-Illia, S. Demoustier-Champagne, P. Audebert, C. Sanchez, Adv. Mater. 15 (2003) 217;
(b) E.L. Crepaldi, G.J. de, A.A. Soler-Illia, D. Crosso, F. Cagnol, F. Ribot, C. Sanchez, J. Am. Chem. Soc. 125 (2003) 9786;
(c) H. Fujii, M. Ohtaki, K. Eguchi, J. Am. Chem. Soc. 120 (1998) 6832.

[14] (a) N. Steunou, F. Ribot, K. Boubekeur, J. Maquet, C. Sanchez, New J. Chem. 23 (1999) 1079;
(b) V.W. Day, T.A. Eberspacher, W.G. Klemperer, C.W. Park, J. Am. Chem. Soc. 115 (1993) 8469;
(c) V.W. Day, T.A. Eberspacher, Y. Chen, J. Hao, W.G. Klemperer, Inorg. Chim. Acta 229 (1995) 391;
(d) N. Steunou, F. Robert, K. Boubekeur, F. Ribot, C. Sanchez, Inorg. Chim. Acta 279 (1998) 144;
(e) C.F. Campana, Y. Chen, V.W. Day, W.G. Klemperer, R.A. Sparks, J. Chem. Soc. Dalton Trans. (1996) 691;
(f) N. Steunou, G. Kickelbick, K. Boubekeur, C. Sanchez, J. Chem. Soc. Dalton Trans. (1999) 3653.

[15] (a) R. Schmid, A. Mosset, J. Galy, J. Chem. Soc. Dalton Trans. (1991) 1999;
(b) V.W. Day, T.A. Eberspacher, W.G. Klemperer, C.W. Park, F.S. Rosenberg, J. Am. Chem. Soc. 113 (1991) 8190.

[16] (a) G.J. de, A.A. Soler-Illia, E. Scolan, A. Louis, P.A. Albouy, C. Sanchez, New J. Chem. 25 (2001) 156–165;
(b) N. Steunou, S. Froster, P. Florian, C. Sanchez, M. Antonietti, J. Mater. Chem. 12 (2002) 3426.

[17] A. Tuel, L.G. Hubert-Pfalzgraf, J. Catal. 217 (2003) 343.

[18] (a) L. Jun, J.C. Yu, D. Lo, S.K. Lam, J. Catal. 183 (1999) 368;
(b) J.C. Yu, J.G. Yu, W.K. Ho, Z.T. Jiang, L.Z. Zhang, Chem. Mater. 14 (2002) 3808.

[19] G. Busca, G. Ramis, J.M.G. Amores, V.S. Escribano, P. Piaggio, J. Chem. Soc. Faraday Trans. 90 (1994) 3181.

[20] (a) A. Brioude, F. Lequevre, J. Mugnier, J. Dumas, G. Guiraud, J.C. Plenet, J. Appl. Phys. 88 (2000) 6187;
(b) D. Bersani, P.P. Lottici, X.Z. Ding, Appl. Phys. Lett. 72 (1998) 73.

[21] (a) J.C. Yu, W.K. Ho, J.G. Yu, S.K. Hark, K.S. Iu, Langmuir 19 (2003) 3889;
(b) J.C. Yu, J.G. Yu, J.C. Zhao, Appl. Catal. B 36 (2002) 31.

[22] (a) E. Sanchez, T. Lopez, R. Gomez, M.A. Bokhimi, O. Novaro, J. Solid State Chem. 122 (1996) 309;
(b) Z. Ding, G.Q. Lu, P.F. Greenfield, J. Phys. Chem. B 104 (2000) 4815.

[23] (a) C. Wagner, W.M. Riggs, L.E. Davis, J.F. Moulder, G.E. Muilemberg, Handbook of X-ray Photoelectron Spectroscopy, Perkin-Elmer Corp., Eden Prairie, MN, 1979;
(b) D. Briggs, Handbook of X-ray and Ultraviolet Photoelectron Spectroscopy, Heden Ltd, London, 1977.

[24] J.C. Yu, J.G. Yu, H.Y. Tang, L.Z. Zhang, J. Mater. Chem. 12 (2002) 81.

[25] N. Serpone, R.F. Khairutdinov, in: P.V. Kamat, D. Meisel (Eds.), Semiconductor Nanoclusters, Physical, Chemical, and Catalytic Aspects, Elsevier Science, Amsterdam, 1997.